Smc5/6-mediated regulation of replication progression contributes to chromosome assembly during mitosis in human cells

Lina Marcela Gallego-Paez[a,b,c], Hiroshi Tanaka[a], Masashige Bando[a], Motoko Takahashi[c], Naohito Nozaki[d], Ryuichiro Nakato[a], Katsuhiko Shirahige[a,b,e], and Toru Hirota[c]

[a]Research Center for Epigenetic Disease, Institute of Molecular and Cellular Biosciences, University of Tokyo, Tokyo 113–0032, Japan; [b]Department of Biological Sciences and [d]Bio-Frontier Research Center, Tokyo Institute of Technology, Yokohama 226–8501, Japan; [c]Cancer Institute, Japanese Foundation for Cancer Research, Tokyo 135–8550, Japan; [e]Core Research for Evolutional Science and Technology (CREST), Japan Science and Technology Agency, Tokyo 102–0076, Japan

ABSTRACT **The structural maintenance of chromosomes (SMC) proteins constitute the core of critical complexes involved in structural organization of chromosomes. In yeast, the Smc5/6 complex is known to mediate repair of DNA breaks and replication of repetitive genomic regions, including ribosomal DNA loci and telomeres. In mammalian cells, which have diverse genome structure and scale from yeast, the Smc5/6 complex has also been implicated in DNA damage response, but its further function in unchallenged conditions remains elusive. In this study, we addressed the behavior and function of Smc5/6 during the cell cycle. Chromatin fractionation, immunofluorescence, and live-cell imaging analyses indicated that Smc5/6 associates with chromatin during interphase but largely dissociates from chromosomes when they condense in mitosis. Depletion of Smc5 and Smc6 resulted in aberrant mitotic chromosome phenotypes that were accompanied by the abnormal distribution of topoisomerase IIα (topo IIα) and condensins and by chromosome segregation errors. Importantly, interphase chromatin structure indicated by the premature chromosome condensation assay suggested that Smc5/6 is required for the on-time progression of DNA replication and subsequent binding of topo IIα on replicated chromatids. These results indicate an essential role of the Smc5/6 complex in processing DNA replication, which becomes indispensable for proper sister chromatid assembly in mitosis.**

Monitoring Editor
Orna Cohen-Fix
National Institutes of Health

Received: Jan 9, 2013
Revised: Nov 5, 2013
Accepted: Nov 13, 2013

INTRODUCTION

The structural maintenance of chromosomes (SMC) proteins constitute the core of several highly conserved protein complexes with critical roles in chromosome architecture and organization during the cell cycle and are essential elements for the preservation of genomic stability (Hirano, 2002). In eukaryotes, the Smc1/3 heterodimer belongs to the cohesin complex, which ensures the pairing of sister chromatids until they segregate during anaphase (Losada *et al.*, 1998; Toth *et al.*, 1999; Uhlmann *et al.*, 1999, 2000; Sumara *et al.*, 2000), whereas condensin complexes containing the Smc2/4 heterodimer participate in the regulation of mitotic chromosome condensation together with the activity of topoisomerase IIα (topo IIα; Earnshaw *et al.*, 1985; Gasser *et al.*, 1986; Uemura *et al.*, 1987; Hirano and Mitchison 1994; Hirano *et al.*, 1997). A third complex consisting of Smc5/6 heterodimers and several non-SMC elements (Nse1–6) is less well characterized. Some of these Nse proteins, such as Nse1, which contains a RING finger domain typical of ubiquitin ligases, and Mms21/Nse2, which has SUMO ligase activity, provide relevant enzymatic activity (Fujioka *et al.*, 2002; McDonald *et al.*, 2003; Morikawa *et al.*, 2004; Pebernard *et al.*, 2004; Zhao and Bobel, 2005).

This article was published online ahead of print in MBoC in Press (http://www.molbiolcell.org/cgi/doi/10.1091/mbc.E13-01-0020) on November 20, 2013.

Address correspondence to: Katsuhiko Shirahige (kshirahi@iam.u-tokyo.ac.jp) or Toru Hirota (thirota@jfcr.or.jp).

Abbreviation used: CREST, autoimmune syndrome characterized by calcinosis, Raynaud's phenomenon, esophageal dysfunction, sclerodactyly, and telangiectasis.

In budding yeast, all components of the Smc5/6 complex are essential for cell viability (Verkade *et al.*, 1999; Harvey *et al.*, 2004), and epistasis analysis with the Rad51 protein indicates the Smc5/6 complex participates in several aspects of double-strand break repair by the homologous recombination pathway (Lehmann *et al.*, 1995; McDonald *et al.*, 2003; De Piccoli *et al.*, 2006). These functions have been corroborated in other species (Potts *et al.*, 2006; Chiolo *et al.*, 2011; Stephan *et al.*, 2011; Wu *et al.*, 2012). However, relatively little is known about the involvement of the complex in general chromatin organization in the absence of DNA damage. A recent study highlighted the important contribution of the Smc5/6 complex, specifically of the Mms21 SUMO ligase activity, to the resolution of a variety of DNA-mediated linkages arising not only in the context of DNA repair but also during DNA replication (Bermúdez-López *et al.*, 2010). Gross chromosome missegregation can occur if those abnormally linked structures are not efficiently removed prior to anaphase. Regions of DNA containing repetitive sequences, such as ribosomal DNA loci and telomeres, have consistently been shown to become highly unstable in yeast Smc5/6 mutants as a consequence of incomplete replication and the persistence of DNA linkages that ultimately result in chromosome breakage (Torres-Rosell *et al.*, 2005, 2007, Bermúdez-López *et al.*, 2010; Chavez *et al.*, 2010). Interestingly, chromatin immunoprecipitation-sequencing (ChIP-Seq) analysis in *Saccharomyces cerevisiae* revealed that the frequency of chromosomal association sites of the Smc5/6 complex increases in response to increased superhelical tension caused by chromosome lengthening, chromosome circularization, or inactivation of topo IIα. This has been proposed to reflect the requirement of Smc5/6 for preventing the accumulation of positive supercoiling ahead of the replication machinery by promoting replication fork rotation on a chromosome scale at sites of sister chromatid intertwining (Kegel *et al.*, 2011). Although this model implies the possible roles of Smc5/6 function in chromosome maintenance in yeast, it remains to be determined to what extent the complex exerts these structural roles in higher eukaryotes, which contain longer and more-complex chromatin.

In this study, we analyzed the cell cycle profile of the human Smc5/6 complex and its contribution to chromosome structure under physiological unperturbed conditions. Smc5 and Smc6 associate with chromatin during interphase and largely dissociate during mitosis, in a manner similar to that of the human cohesin complex. Interestingly, depletion of Smc5 and Smc6 results in aberrant mitotic chromosomal structures and impaired chromosomal axial localization of topo IIα and the condensin Smc2. Moreover, a detailed analysis of chromosome structure during interphase by premature chromosome condensation (PCC) assay revealed that a perturbed progression of replication after Smc5/6 depletion interferes with the timing of topo IIα binding and relocalization onto chromosomes before cells enter mitosis, suggesting an essential role for the Smc5/6 complex in linking DNA replication with higher-order chromatin structure.

RESULTS

Localization of Smc5 and Smc6 during the cell cycle

To examine the localization of the Smc5/6 complex during the cell cycle, we first analyzed the immunostaining pattern of Smc5 in fixed human RPE-1 cells. The protein appeared predominantly in the nucleus during interphase. In mitotic cells, Smc5/6 was found diffusively in the cytoplasm and excluded from chromosomes. When cells were briefly treated with a detergent before the fixation, following the preextraction protocol, Smc5/6 was seen to associate with the chromatin during interphase and to dissociate from mitotic chromosomes, until G_1 phase, when its nuclear staining was visible again (Figure 1A and Supplemental Figure S1C). Live-cell imaging of HeLa cells stably expressing enhanced green fluorescent protein (EGFP)-tagged Smc5 was consistent with these immunofluorescence observations (Figures 1B and S1, A, B, and D). In addition, whole-cell lysates were prepared from RPE-1 cells arrested at G_2 by treatment with an ATP-competitive inhibitor of Cdk1, RO-3306, and were subjected to chromatin fractionation and immunoblotting (Figure 1C). Smc5 and Smc6 were found primarily in the chromatin fraction under these conditions. However, when the cells were allowed to proceed into mitosis and were then arrested by treating them with *S*-trityl-L-cysteine (STLC, a potent inhibitor of Eg5 that causes monopolar spindles; DeBonis *et al.*, 2004), a substantial proportion of the Smc5 and Smc6 proteins moved to the cytoplasmic fraction. This behavior of the Smc5/6 complex implies that it is involved in the maintenance of chromatin structure primarily during interphase.

Abnormal chromosome morphology in Smc5- and Smc6-depleted cells

To gain insight into the function of the human Smc5/6 complex beyond the context of DNA repair, we suppressed the expression of Smc5 or Smc6 in RPE-1 cells by transfecting small interfering RNAs (siRNAs) specific to Smc5 and Smc6 (Figure 2). More than 80% of Smc5 or Smc6 protein was depleted after two rounds of transfection (72 h in total). Depletion of Smc5 caused a decrease in the Smc6 protein levels and vice versa, consistent with the idea that these proteins are stable as a protein complex (Figure 2A). Immunofluorescence microscopy also verified the reduction of Smc5 or Smc6 staining in cells treated with their specific siRNAs (Figure S2A).

Next we examined whether depletion of Smc5 and Smc6 affects the structure of mitotic chromosomes. Smc5 and Smc6 siRNA–treated RPE-1 cells exhibited a lower proliferation rate than control cells (Figure S2B). We then depleted Smc5 and Smc6 in cells arrested in mitosis, and the morphology of chromosomes was examined by spreading and Giemsa staining (Figures 2, B–E, and S3, A–C). In control cells, chromosomes showed characteristic rod-shaped structure and sister chromatids remained tightly connected at centromeres. In Smc5- and Smc6-depleted cells, however, a high proportion of metaphase cells exhibited an abnormal chromosomal conformation characterized by a "curly" appearance. A subpopulation of these cells contained unevenly condensed chromosomes that revealed low levels of condensation at centromeres with higher levels at distal arms. In addition, ~25% of chromosomes exhibiting the curly phenotype also showed a cohesion defect (Figures 2, B and E, and S3, A and C). Furthermore, Smc5- and Smc6-depleted cells frequently generated lagging chromosomes and/or anaphase bridges. The majority of the latter were positive for Plk1-interacting checkpoint helicase (PICH) and Bloom syndrome helicase (BLM) (Figure 3, A–E), indicating that they mainly represent centromeric unwound catenane structures (Baumann *et al.*, 2007; Rouzeau *et al.*, 2012). Moreover, immunostaining of centromeric antigens by autoimmune syndrome characterized by calcinosis, Raynaud's phenomenon, esophageal dysfunction, sclerodactyly, and telangiectasis (CREST) antisera indicated that postmitotic micronuclei were formed that contained single or multiple chromosome fragments (Figure 3B), suggesting chromosome loss/breakage occurred during cell division. Thus the function of Smc5 and Smc6 during interphase appeared to be essential for proper chromosome assembly and segregation in subsequent mitosis.

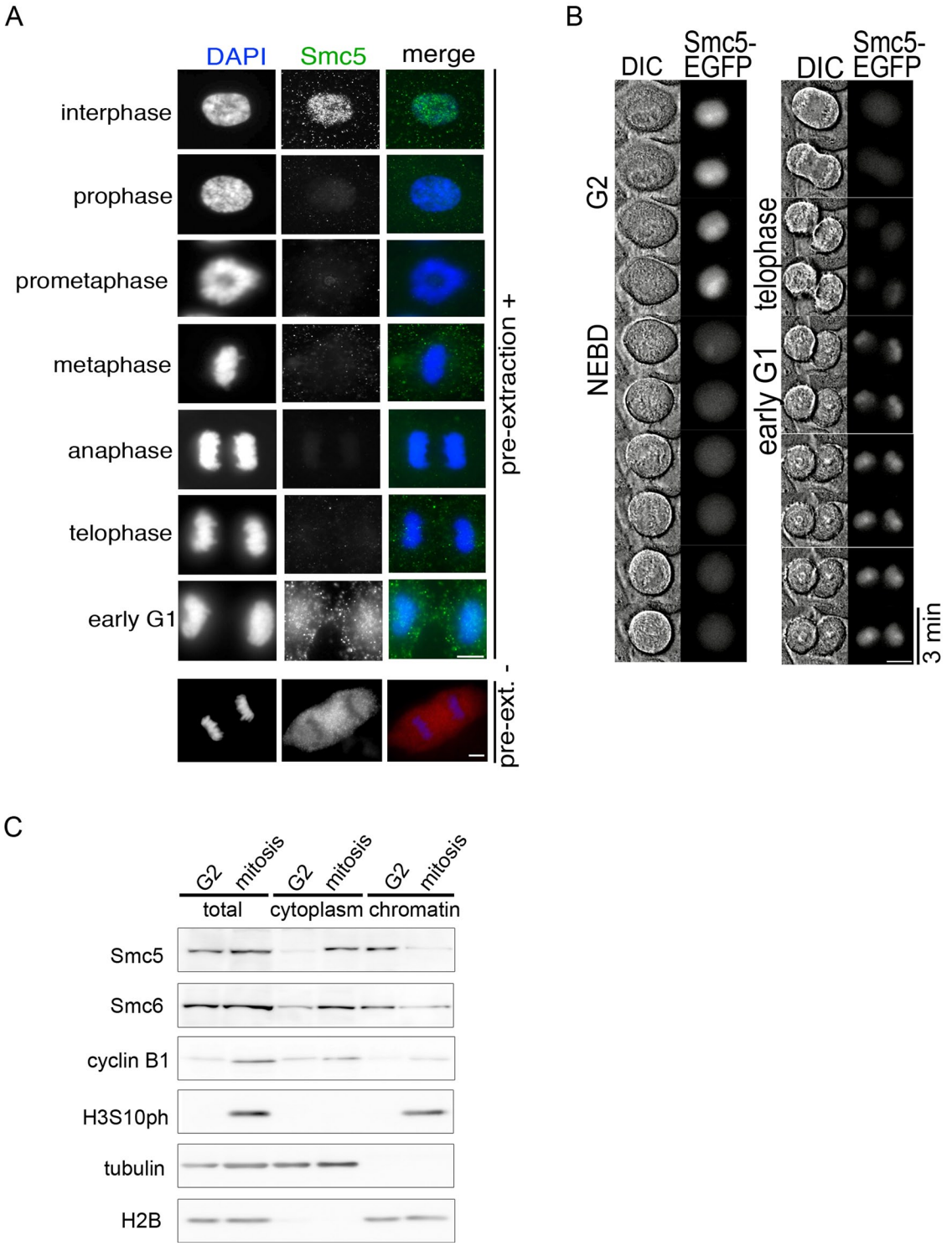

FIGURE 1: Chromatin association of the Smc5/6 complex during the cell cycle. (A) RPE-1 cells with or without preextraction with 0.2% PBS/Triton X-100 were fixed in paraformaldehyde and stained with Smc5 antibody. DNA was stained with DAPI. Merged images contain Smc5 (green) and DAPI staining (blue). Scale bar: 10 μm. (B) Cell cycle behavior of Smc5 analyzed by live-cell imaging. Time-lapse images of HeLa cells stably expressing EGFP-Smc5 were acquired at 3-min intervals. Fluorescence and differential interference contrast images are shown for each time point. NEBD indicates nuclear envelope breakdown. Scale bar: 10 μm. (C) RPE-1 cells arrested at G_2 by treatment with RO-3306 and cells enriched in mitosis by STLC treatment after release from G_2 arrest were subjected to chromatin fractionation and immunoblotting. Relative intensity of Smc5 and Smc6 bands indicated in total and cytoplasmic fractions and in chromatin fractions were normalized by tubulin and histone H2B levels, respectively. Expression of cyclin B1 and phosphorylation of H3 (H3S10ph) were used as markers for mitosis.

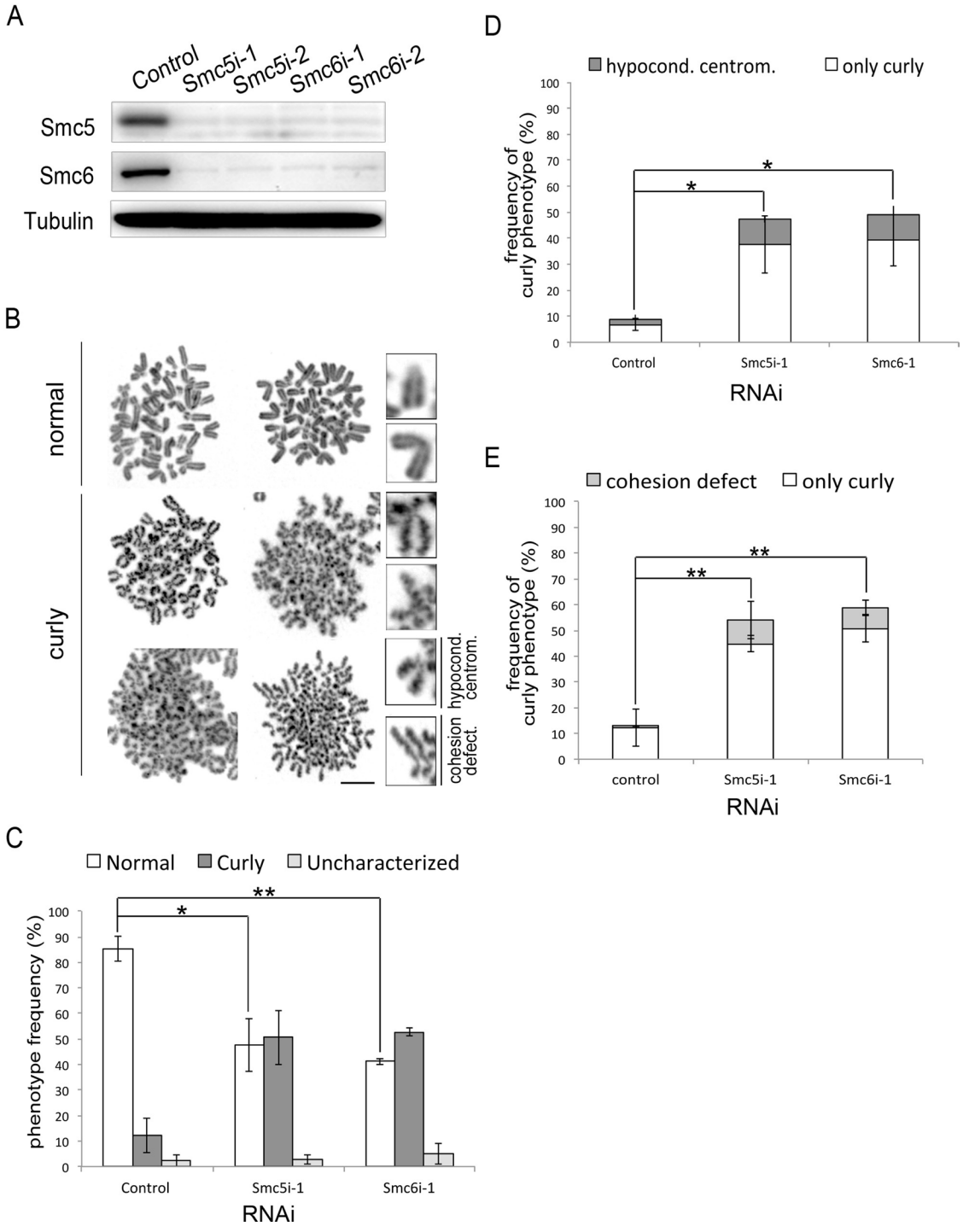

FIGURE 2: RNAi-mediated depletion of Smc5 and Smc6 in RPE-1 cells. (A) Logarithmically proliferating RPE-1 cells were transfected with the indicated siRNA, and WCE were analyzed by immunoblotting 72 h after the transfection. Tubulin staining was shown as a loading control. Note that Smc6 becomes unstable in Smc5-depleted cells, and vice versa. (B) RPE-1 cells transfected with siRNAs against Smc5 or Smc6 were synchronized by serum starvation for 144 h, allowed to recover in serum-containing medium, and then treated with STLC to induce arrest in mitosis. Cells were harvested, and Giemsa-stained chromosome spreads were prepared. Scale bar: 10 μm. (C) Incidence of mitotic cells with curly chromosomes in cells transfected with indicated siRNAs. (D and E) Additional defects observed within the curly chromosomes in cells depleted of Smc5 or Smc6. Proportion of cells with hypercondensation of distal arms (D) and those with cohesion defect (E) are shown in the histogram. For (C–E), 300 cells per indicated condition were examined. Bar graph shows mean ± SD from three independent experiments; p value < 0.05; *, $p = 0.01–0.05$; **, $p = 0.001–0.01$; two-tailed Student's t test.

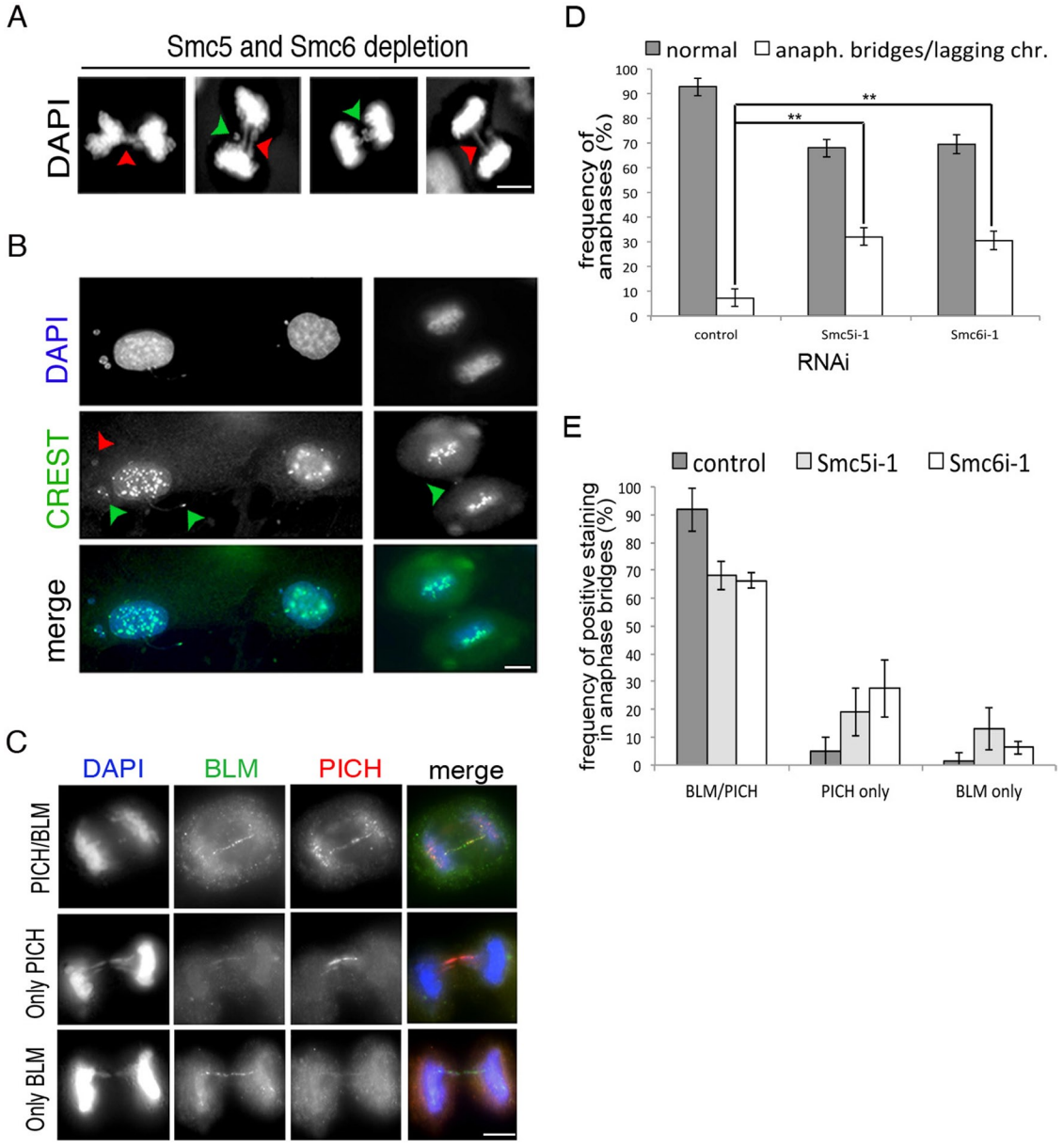

FIGURE 3: Depletion of Smc5 or Smc6 disrupts chromosome segregation. (A) Example images of the anaphase bridges (red arrowheads) and lagging chromosomes (green arrowheads) frequently seen in Smc5/6-depleted cells. Scale bar: 10 μm. (B) Examples of the formation of micronuclei in Smc5- and Smc6-depleted cells. Green arrows indicate micronuclei containing the centromere marker CREST; red arrows indicate micronuclei negative for the CREST signal. Scale bar: 10 μm. (C) Representative images of PICH (red) and BLM (green) immunofluorescence in anaphase bridges. DNA was counterstained with DAPI (blue). Scale bar: 10 μm. (D) Frequency of anaphase bridges and lagging chromosomes within the anaphase chromosomes observed in the control and siRNA-treated cells. Three hundred anaphases were analyzed per condition. Bar graph shows mean ± SD from three independent experiments; p value < 0.05; **, $p = 0.001$–0.01; two-tailed Student's t test. (E) Frequency of anaphase bridges positive for PICH and BLM, PICH only, or BLM only. One hundred anaphase bridges were analyzed for each sample.

Defective axial localization of topo IIα and condensin in the absence of the Smc5/6 complex

The abnormal chromosome morphology observed in Smc5- and Smc6-depleted cells prompted us to consider the possibility that this curly chromosome conformation reflects a deficiency in higher-order chromatin structure. Topo IIα and the two condensin complexes present in humans (condensin I and condensin II) are the main constituents of the so-called dynamic "chromosome scaffold" and colocalize at the axes of metaphase chromatids (Earnshaw *et al.*, 1985; Gasser *et al.*, 1986; Hirano *et al.*, 1997; Maeshima and Laemmli, 2003). Thus we examined the binding pattern of topo IIα and Smc2 (a common component of both condensin complexes) in chromosome spreads by immunofluorescence microscopy (Figures 4, 5, and S3, F and G). Staining in the control cells showed a normal beaded/coil-like pattern along the axis of each chromatid, with an intense signal of topo IIα concentrated at the centromeres, as characterized. However, both Smc5- and Smc6-depleted cells showed an abnormal distribution of topo IIα along the chromosome axis that resembled the curly appearance of chromatids observed in Giemsa staining (Figures 4, A–C,

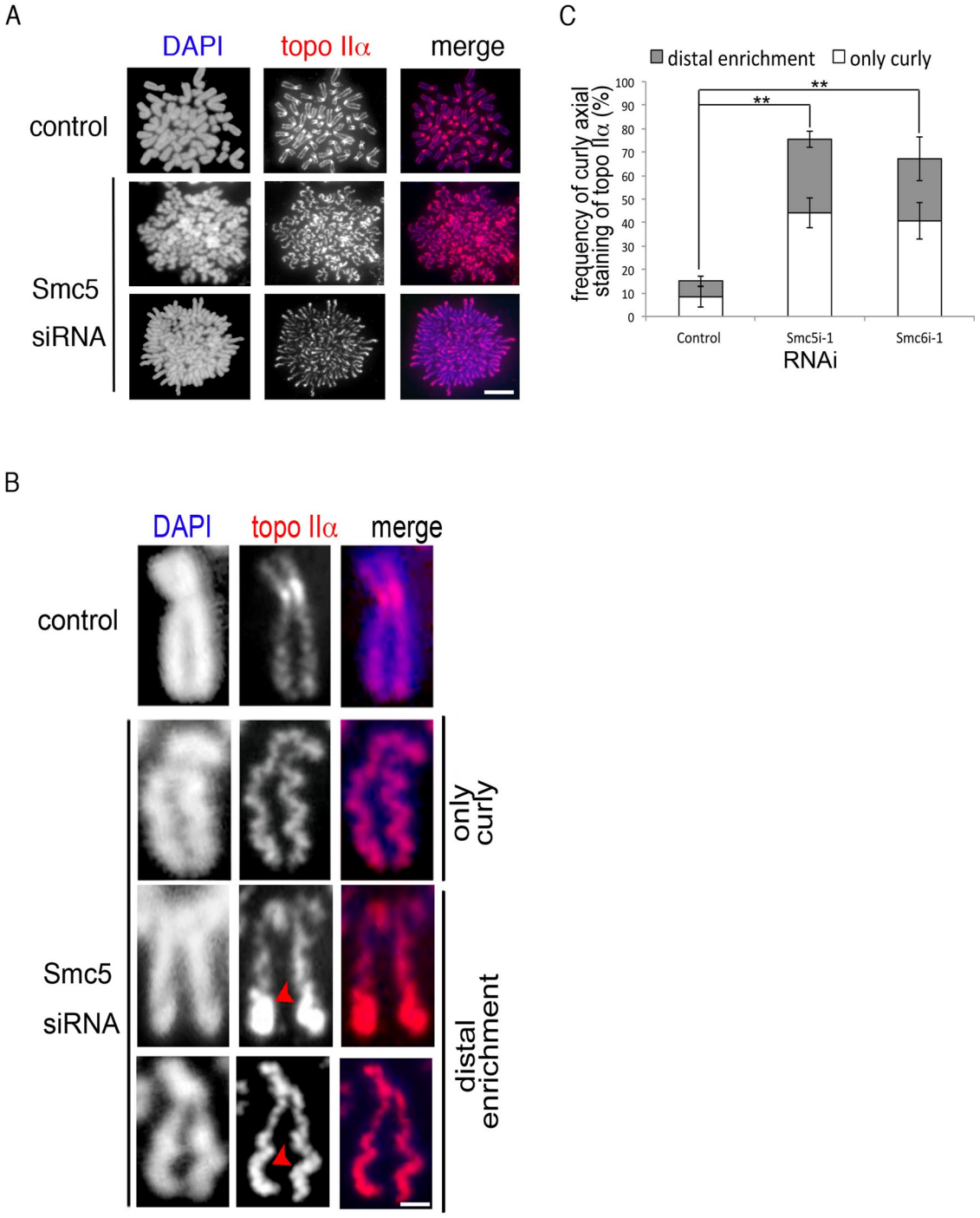

FIGURE 4: Chromosome axis deformation in Smc5/6-depleted cells. (A) RPE-1 metaphase cells transfected with siRNAs against Smc5 or Smc6 or a control mock were subjected to hypotonic treatment, fixation, and staining for DNA (DAPI) and topo IIα. Right panels show the merged images of DAPI (blue) and topo IIα (red). Scale bar: 5 μm. (B) Examples of individual chromosome morphologies observed in control and Smc5-depleted cells. In merged images in the right panels, DAPI staining is shown in blue and topo IIα in red. Red arrowheads point to the defects mentioned. Scale bar: 1 μm. (C) Frequency of curly axial staining of topo IIα with or without enrichment at distal chromosome regions. Three hundred metaphases were analyzed for each sample. Bar graph shows mean ± SD from three independent experiments; p value < 0.05; **, $p = 0.001–0.01$; two-tailed Student's t test.

and S3, D and E). Strikingly, the centromeric enrichment of topo IIα was apparently reduced in these curly chromosomes. Instead, topo IIα enrichment was seen on distal arms, increasingly toward the ends and typically in unevenly condensed chromosomes (Figure 4, B and C).

Next we analyzed the chromosomal localization of Smc2 and found that depletion of Smc5 and Smc6 led to an irregular distribution of Smc2 along the chromatid lengths with ill-defined axial structure (Figures 5, A–E, and S3F). A series of three-dimensional reconstitution images further depicted the aberrant

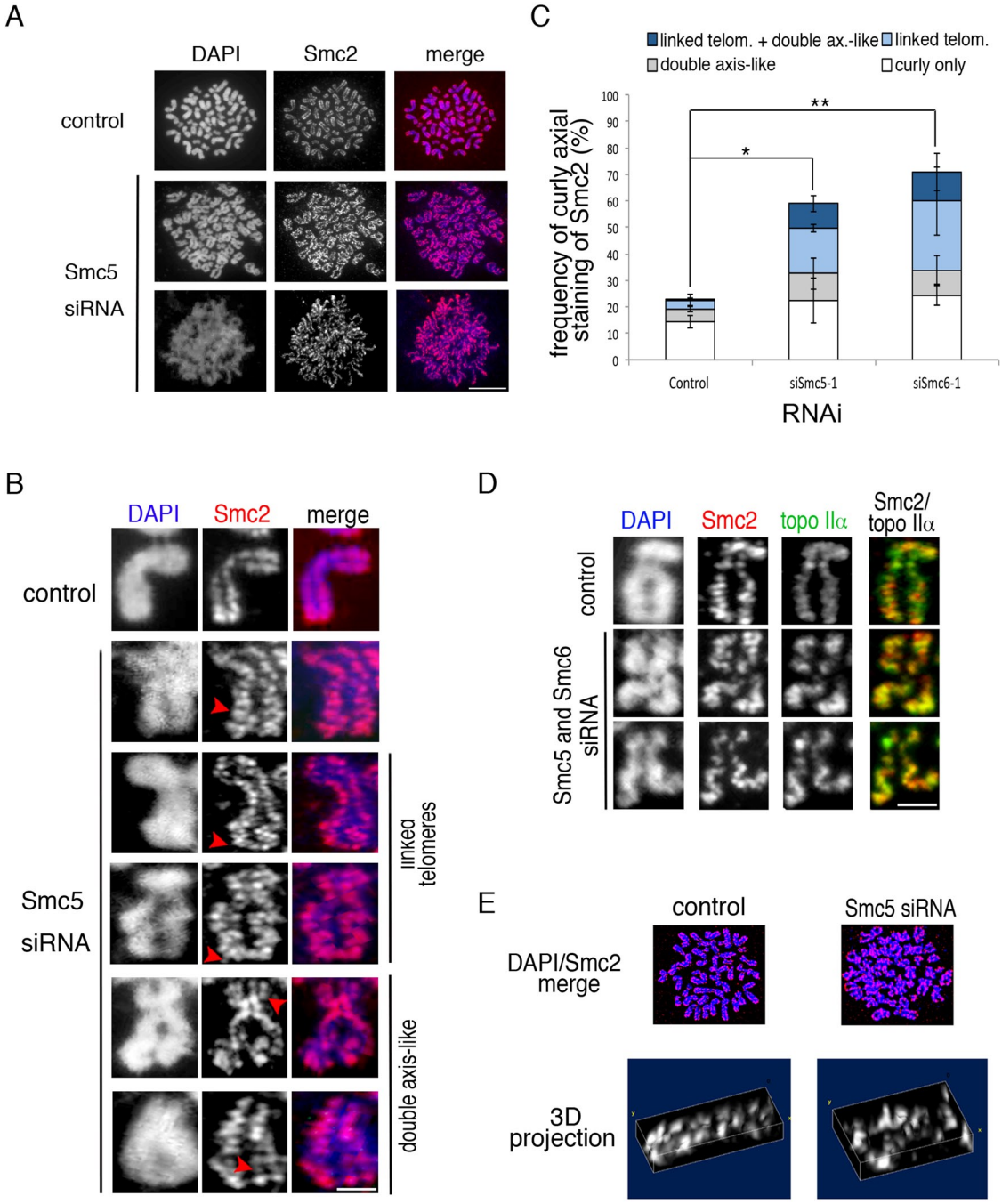

FIGURE 5: (A) Metaphase chromosome spreads were prepared from control and Smc5-depleted cells and stained with DAPI (blue) and anti-Smc2 (red). Scale bar: 5 μm. (B) Images of individual chromosomes showing the linked telomeres and "double axis–like" staining observed in the Smc5/6-depleted cells. Smc2 staining is in red, and DAPI in blue. Scale bar: 1 μm. (C) Frequency of disorganized axial Smc2 staining (white) or with at least one chromosome with additional double axis–like staining (gray), linked telomeres (light blue), or a combination of both linked telomeres and "double axis-like" staining (dark blue). Three hundred metaphases were analyzed for each sample. Bar graph shows mean ± SD from three independent experiments; p value < 0.05; *, p = 0.01–0.05; **, p = 0.001–0.01; two-tailed Student's t test. (D) Representative examples of chromosomes observed in metaphase spreads from control and Smc5- or Smc6-depleted cells stained with DAPI, Smc2, and topo IIα, as indicated. In merged images, Smc2 is shown in red and topo IIα in green. Note that the characteristic barber pole–like alternate pattern of topo IIα and Smc2 distribution in control cells contrasts with the irregular distribution in Smc5/6-depleted cells. Scale bar: 1 μm. (E) Three-dimensional reconstruction of the Smc2 staining of metaphase chromosomes in the Smc5/6-depleted cells.

distribution of condensin in Smc5/6-depleted cells (Figure 5E). In some cases, the telomeric staining of Smc2 appeared to be connected between the sister chromatids, generating "closed" chromosomes (Figures 5, B and C, and S3F). Enigmatically, some chromatids with the intense distal staining showed a double axis–like staining for Smc2, particularly in chromosomes

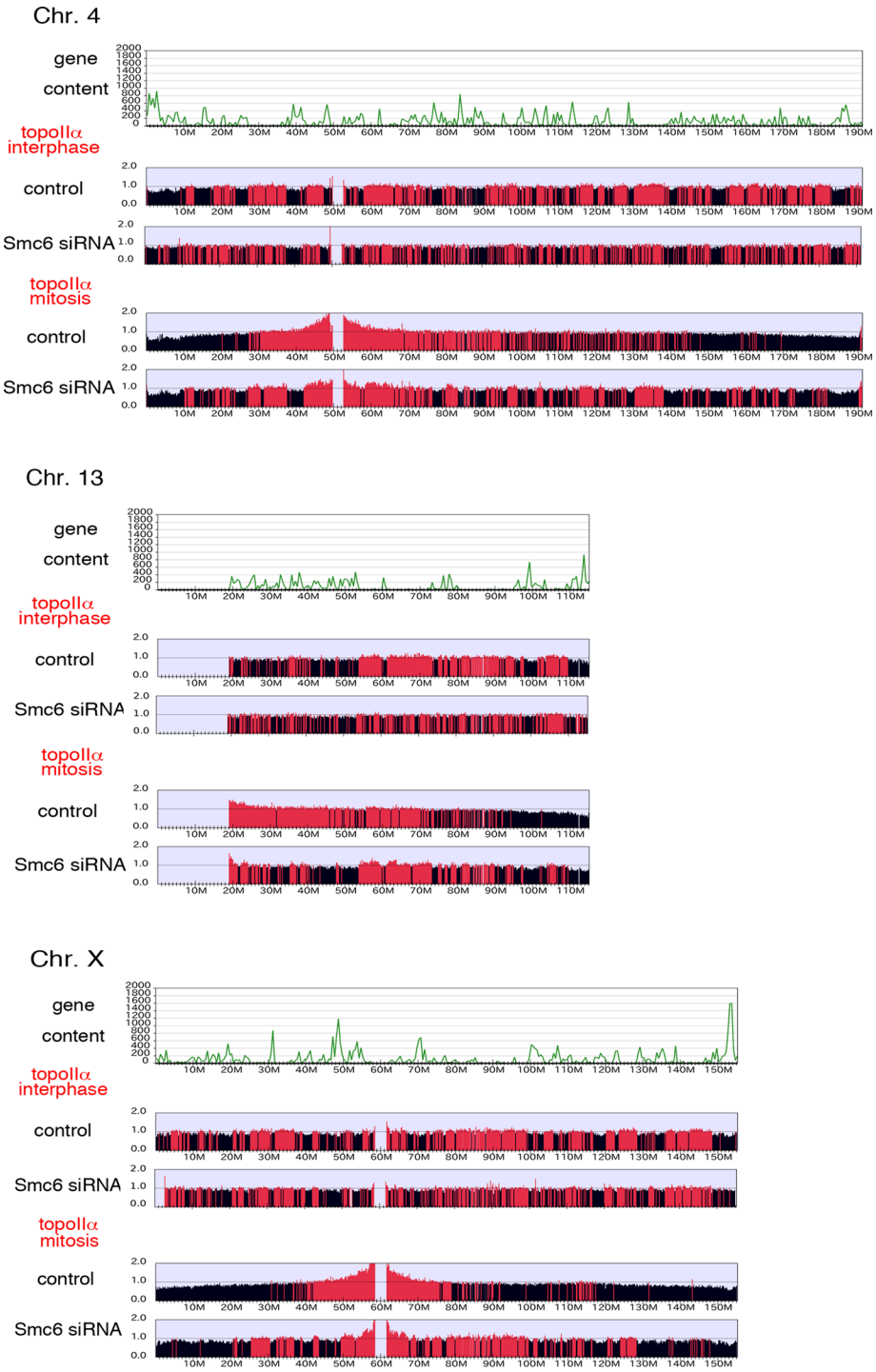

FIGURE 6: Chromatin binding profile of topo IIα on human chromosomes in interphase and mitosis in the presence and absence of Smc6, as revealed by ChIP-Seq. Uniquely aligned reads are summed in 100-kb windows along the chromosome for ChIP fractions and WCE. Windows in which the enrichment ratio of ChIP/WCE was higher than 1.0 are highlighted in red (see *Materials and Methods*). Gene content was calculated for every 500 kb. Representative results for chromosomes 4, 13, and X are shown; these exemplify the requirement of Smc5/6 for the timed binding of topo IIα in interphase and the relocalization of topo IIα in mitosis.

with the hypocondensed centromere phenotype (Figure 5, B and C).

Furthermore, when the structure of the chromosomal axis was examined by double staining for topo IIα and Smc2, the characteristic barber pole–like alternate distribution of these proteins (Maeshima and Laemmli, 2003) was frequently disrupted in Smc5- and Smc6-depleted cells (Figure 5D). Together these results strongly suggest that, as is the case for other Smc-containing complexes, the Smc5/6 complex is crucial for mitotic chromosome assembly, and the cellular localization of the complex argues a specific role for this complex during interphase.

Topo IIα mislocalization upon Smc6 depletion during mitosis

To better understand the role of Smc5/6 in the genome-wide profile of topo IIα localization, we performed ChIP-Seq analysis of asynchronous and mitotic arrested HeLa cells transfected with control or Smc6 siRNA (Figure 6). In the asynchronous sample, topo IIα localized to binding sites along the entire length of the chromosomes, with an apparent accumulation at regions of low gene density. Topo IIα binding profiles changed dramatically once cells entered mitosis. Most topo IIα concentrated at the centromeric and pericentromeric regions and substantially decreased its binding along the arms and telomeric regions, in agreement with immunofluorescence microscopy (Figure 4, A and B). Strikingly, while interphase localization pattern of topo IIα did not present important changes, apart from a mild decrease in the overall chromosomal enrichment in Smc6-depleted cells, topo IIα did show a markedly different mitotic chromatin-binding profile from that seen in control cells. Topo IIα enrichment at the centromeric/pericentromeric region was reduced in Smc6-depleted cells, and the general redistribution of topo IIα did not appear to take place, as most of the binding along the arms resembled the pattern observed in asynchronous cultured cells. Thus the Smc5/6 complex is required for topo IIα chromosomal distribution during mitosis, which seems essential for proper axial conformation and general chromosome architecture.

Perturbed replication upon Smc5/6 depletion affects binding of topo IIα to chromatin during interphase

The findings that mitotic chromosome structure became defective without normal levels of Smc5/6 and that the bulk of this complex is unloaded from mitotic chromosomes led us to hypothesize that Smc5/6 function in interphase may determine chromosome organization later in mitosis. It has been proposed that a major determinant of the mitotic lethality of Smc5 and Smc6 mutants in fission yeast is defective cohesin removal from chromosome arms, which could reflect abnormal chromatin-binding dynamics of cohesin during interphase (Outwin *et al.*, 2009). However, we did

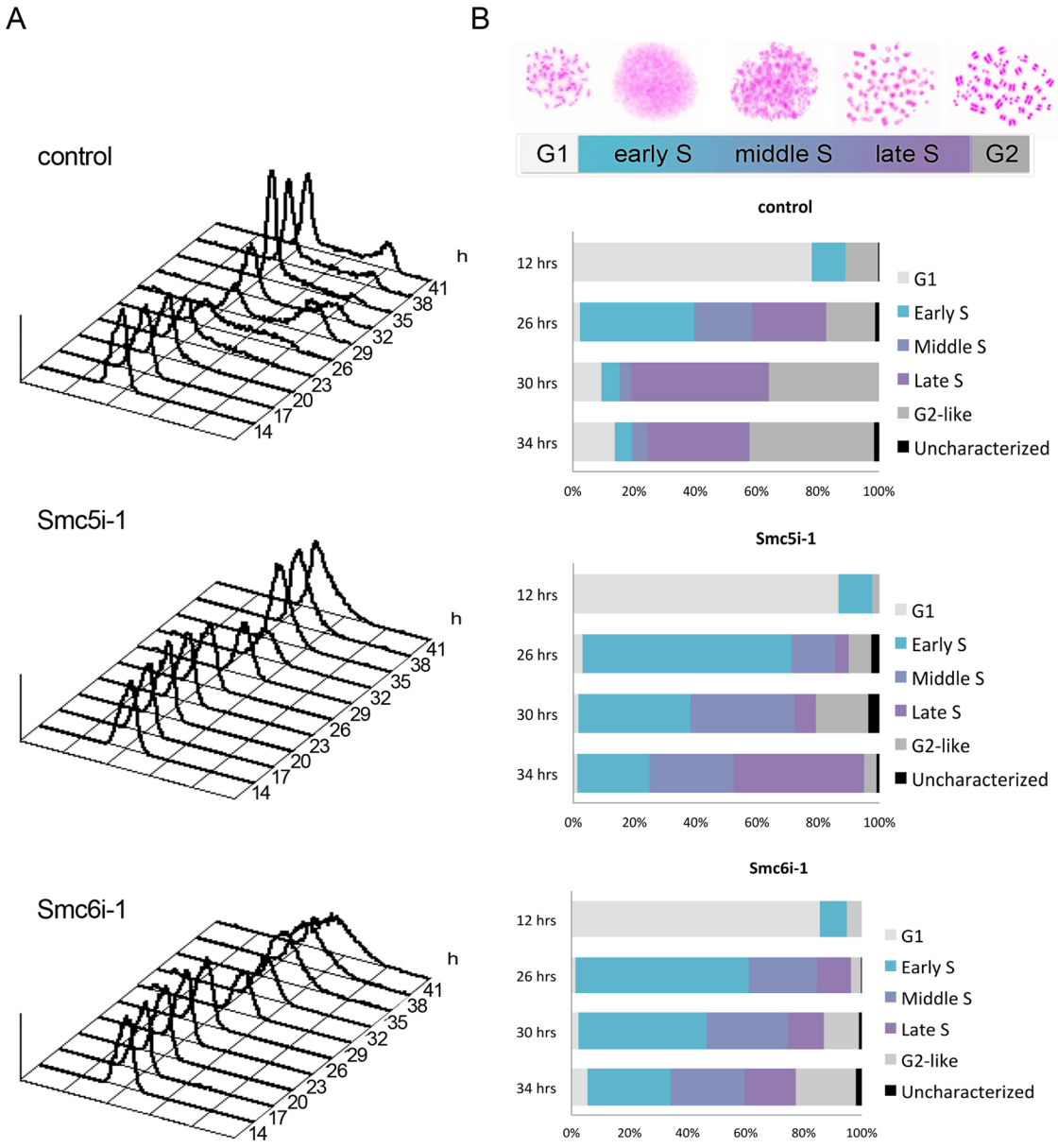

FIGURE 7: Probing different stages of DNA replication using FACS and PCC assay. (A) RPE-1 cells transfected with an siRNA against Smc5 or Smc6 or a control mock were collected at indicated time points after release from serum starvation, and cell cycle distribution was determined by flow-cytometric analysis of DNA content. (B) PCC-induced nuclei from RPE-1 cells transfected with an siRNA against Smc5 or Smc6 or a control mock were treated with hypotonic buffer, fixed, spread on glass slides, and stained with Giemsa solution. Representative images for indicated cell cycle stages are shown. The band graphs represent the average proportion of cells at different interphase stages in control or siRNA-treated samples at the indicated time points after the release from serum starvation between three independent experiments.

not detect any persistent binding of cohesin on mitotic chromosomes after depletion of Smc5/6 in human cells (Figure S4), indicating the abnormal mitotic phenotype in fission yeast seems mechanistically different from the chromosomal structural defect we observed in human cells.

We did observe, however, that cell cycle progression and mitotic entry were delayed in Smc5/6 siRNA–treated cells and that the emergence of cells positive for 5-ethynyl-2′-deoxyuridine (EdU) incorporation, which indicates nascent DNA during replication, was also reduced (Figure S5A). We then directly analyzed cell cycle progression by flow cytometry (Figure 7A). Cells were treated with siRNA during serum starvation (Figure S5B), and synchronous cell populations were analyzed for their DNA content every 3 h. Cells depleted of Smc5 or Smc6 showed significant delay in the progression of DNA synthesis by 2.5-fold when compared with the controls.

What causes the delay in DNA replication in Smc5/6-deficient cells? In yeast, the Smc5/6 complex has been implicated in the stabilization of stalled replication forks and the restart of collapsed replication forks (Ampatzidou *et al.*, 2006; Irmisch *et al.*, 2009), raising the possibility that this complex may have a similar if not identical role in human cells. Moreover, preventing DNA replication perturbs

the formation of topo IIα–containing axes and alters the chromatin-binding properties of topo IIα (Cuvier and Hirano, 2003). Given that Smc5/6 is required for the relocalization of topo IIα (Figure 6), a plausible following question was whether the role of Smc5/6 in regulating replication fork processing is functionally related to behavior of topo IIα during interphase and/or later in mitosis.

We first examined the extent of replication-related DNA damage in Smc5/6-depleted cells by looking at γH2AX and BLM foci, which are formed at stalled and/or collapsed replication fork sites (Davalos and Campisi, 2003; Li *et al.*, 2004; Shimura *et al.*, 2008; Figure 8, A–C). A time-course analysis during the S and G_2 phases indicated no obvious enrichment of γH2AX and BLM foci in the control cells at any time point analyzed. By contrast, Smc5/6-depleted cells showed marked and progressive increase in foci formation, which is indicative of stalled or collapsed replication forks.

To gain insight about the stage of DNA synthesis at which this delay is taking place and to characterize the structural details of the deficient replication progression in the absence of Smc5/6, we subsequently subjected cells released from serum starvation to PCC assay. By treating cells with calyculin A, an inhibitor of type 1 and 2A protein phosphatases that induces PCC, we were able to differentiate the cells from early to late S phase (Figure 7B). In controls, at 12 h after release from serum starvation, almost all cells exhibited characteristic G_1-like chromosomes; at 26 h, the majority of control cells started to accumulate nuclei exhibiting DNA replication, particularly at middle and late S phase, or they contained fully replicated G_2-like chromosomes; by 30 h, the G_2-like and late S-phase nuclei represented the majority of the population. In contrast, Smc6 siRNA–treated cells showed almost no accumulation of G_2-like nuclei, even at 26 h; instead, the nuclei at this time point exhibited a variety of DNA replication stages, from early to late S phase, and had only started to generate G_2-like chromosomes at 30 h. At 34 h after the release, a significant proportion of Smc5/6-depleted cells were still undergoing DNA replication (Figure 7B).

These data indicated that, in the absence of the Smc5/6 complex, DNA replication progresses at a much slower rate, with a concomitant generation of replication-related DNA damage. Importantly, when Smc5/6-depleted cells were treated with RO-3306 at 30 h after release from serum starvation to arrest cells in G_2 for an additional 12 h, most of the γH2AX/BLM foci disappeared, and the incidence of the curly chromosome phenotype and the abnormal axial staining of topo IIα were markedly reduced after release from RO-3306 treatment (Figure 8, C–E). It is reasonable to predict that the abnormal chromosome structure could be rescued by providing the cells more time to deal with the perturbed replication fork progression that occurred during S phase.

Finally, we analyzed the pattern of topo IIα chromatin localization with respect to ongoing replication by immunostaining topo IIα in cells pulse-labeled with EdU for 0.5 h prior to PCC induction (Figure 9, A–C). Both control and Smc6-depleted cells showed a largely similar pattern of topo IIα and EdU staining in PCC-induced nuclei at early and middle S phase, with a characteristic progressive accumulation of topo IIα at particular chromatin domains that were, with rare exceptions, exclusive of EdU-positive nascent replicating chromatin regions. In late S and G_2 nuclei, however, several differences were observed between control and Smc5/6-depleted cells. First, in the absence of Smc5/6, there was a marked accumulation of late S-phase nuclei having a distinctive pattern of EdU and topo IIα staining, and less-defined individual sister chromatids masses were formed, coinciding with a more dispersed pattern of topo IIα. Additionally, EdU-positive chromatin was found as linear staining in between these chromosome structures, a pattern also barely seen in control S-phase nuclei (Figure 9, A and C).

Second, G_2 chromosome structures in Smc5/6-depleted cells showed a high frequency of persistent ongoing replication, while control G_2 nuclei never showed EdU incorporation. This persistent replication was often found at centromeres and telomeres, suggesting that DNA replication was particularly delayed at these sites in the absence of Smc5/6 (Figure 9, B and D). Strikingly, these regions of persistent active replication always excluded topo IIα binding in late S phase, generating an irregular topo IIα staining pattern along G_2 chromosomes. Overall these results indicate that depletion of the Smc5/6 complex markedly retarded S-phase progression, extending the time of DNA replication at particular regions. This delay critically affected the pattern of topo IIα accumulation on PCC chromosomes, and this abnormal binding of topo IIα during replication processes may underlie the abnormal distribution of topo IIα later in mitosis as observed with immunostaining and ChIP-Seq analyses.

DISCUSSION

Regulation of Smc5/6 in time and space

Our study indicates that, in human cells, Smc5/6 associates with chromatin during interphase, but it then largely dissociates from the nucleus in mitosis, consistent with previous analysis (Figure 1; Taylor *et al.*, 2001). In fractionation and immunoblotting analysis, however, we could detect a small amount of Smc5/6 in chromatin-enriched fraction in mitosis (Figure 1C). Consistent with this, when EGFP-Smc5 protein was localized using GFP antibodies, we were able to detect faint signals on mitotic chromosomes (Figure S1D), in agreement with recent observations in mice meiotic cells (Gomez *et al.*, 2013). Thus it would be formally possible to predict that this small fraction of Smc5/6 on chromosomes could account for a minor nuclear function of the complex in mitosis. But in light of our findings, it seems unlikely that this presumed role of Smc5/6 has a more profound effect in mitotic chromosome assembly than its major function, which is associated with replication processing during interphase, when the most abundant association of the complex with chromatin occurs. The observation that the abnormal chromosome structure was rescued by providing extra time before mitosis also supports this view (Figure 8).

Depletion of Smc5 and Smc6 gave rise to a unique mitotic chromosome structure characterized principally by a curly deformation of sister chromatids and hypercondensation of distal arms with concomitant hypocondensation of centromeres (Figure 2). These mitotic phenotypes presumably relate to the function of Smc5/6 during DNA replication, which makes an important contribution to higher-order chromatin organization upon entry into mitosis. Without the function of Smc5/6, chromosomal segregation become defective and often creates PICH- and BLM-positive anaphase bridges that indicate existence of unresolved, intertwining of sister DNAs. As these aberrant phenotypes have also been associated with the loss of topo IIα and condensin function (Gerlich *et al.*, 2006; Spence *et al.*, 2007), delocalization of topo IIα and condensin may be causally related to such segregation defects (Figure 3, B–F).

The behavior of Smc5/6 during the cell cycle in human cells differs from that in yeast or frog (Lindroos *et al.*, 2006; Tsuyama *et al.*, 2006), in that the complex already associates with chromatin in early G_1 phase. This suggests that the Smc5/6 complex is differentially regulated in human cells and has probably acquired additional function before DNA replication. Notably, the localization pattern of Smc5/6 is similar to that of cohesin complex. In light of cohesin's function before S phase (Wendt *et al.*, 2008), Smc5/6 might determine the structure of chromatin to control gene

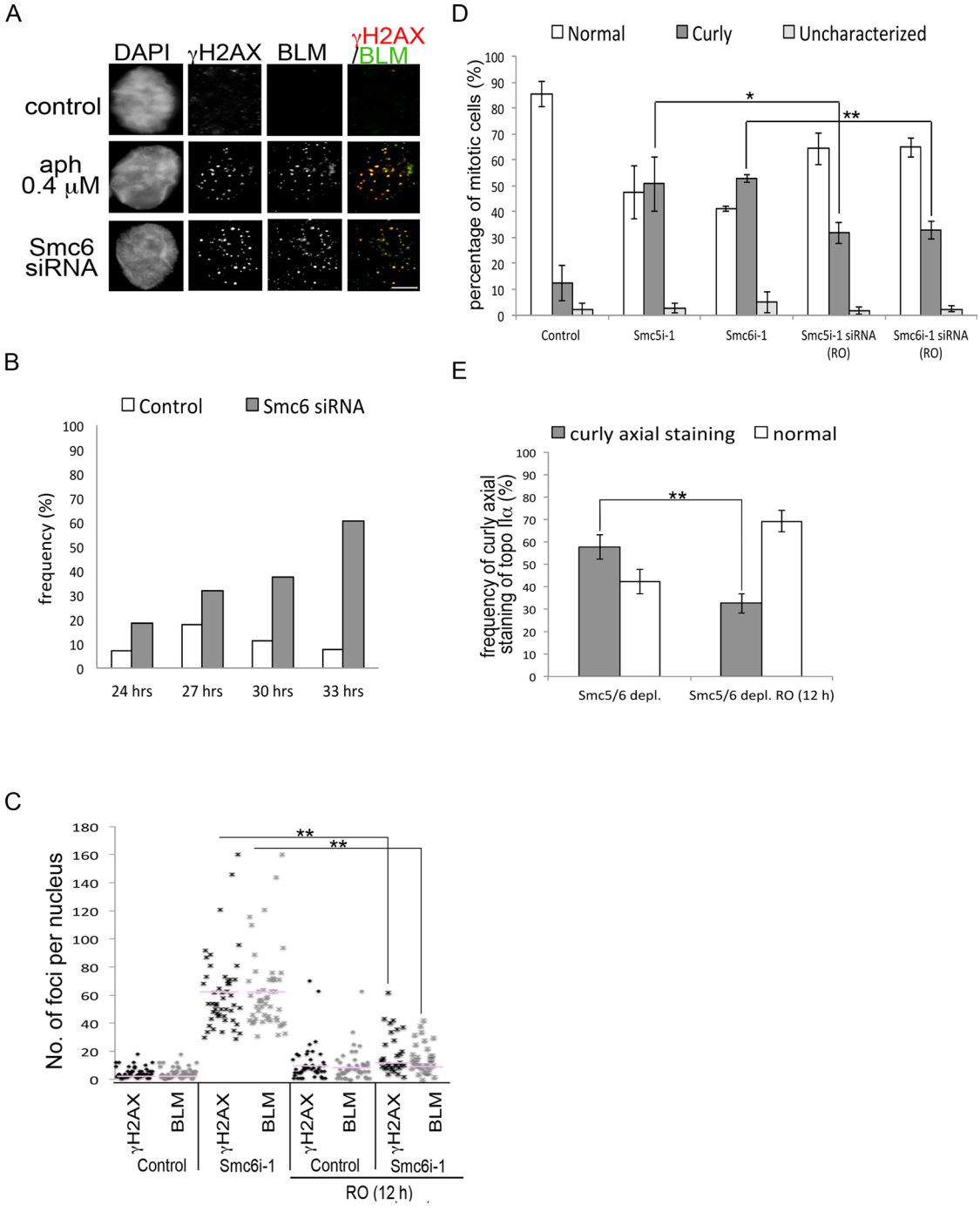

FIGURE 8: Replication-related DNA damage. RPE-1 cells transfected with an siRNA against Smc5 or Smc6 or a control mock were analyzed at the specified time points after release from serum starvation. (A) Representative immunofluorescence of γH2AX (red) and BLM (green) foci formation in control cells (top panels) and in cells depleted of Smc6 (bottom panels). DAPI staining is shown in blue. A positive control for γH2AX and BLM staining is provided by low doze of aphidicolin treatment (aph 0.4 μM; middle panels). Scale bar: 10 μm. (B) Frequency of γH2AX-positive cells at indicated time points after the release from serum starvation. (C) Frequency of γH2AX-positive cells at the 33-h time point, with or without additional RO-3306 treatment for 12 h, and further classified according to the number of foci per cell as indicated ($n > 31$ per condition). Pink bars denote means of foci number per cell. (D) Giemsa-stained spread chromosomes from cells depleted of Smc6 or mock (control) were evaluated for their morphology and are summarized in the histogram. Three hundred cells were examined for each experiment. (E) Frequency of curly axial staining of topo IIα in Smc5/6-depleted cells in the presence or absence of RO-3306 for an additional 12 h. Bar graph shows mean ± SD from three independent experiments; p value < 0.05; *, $p = 0.01–0.05$; **, $p = 0.001–0.01$; two-tailed Student's t test.

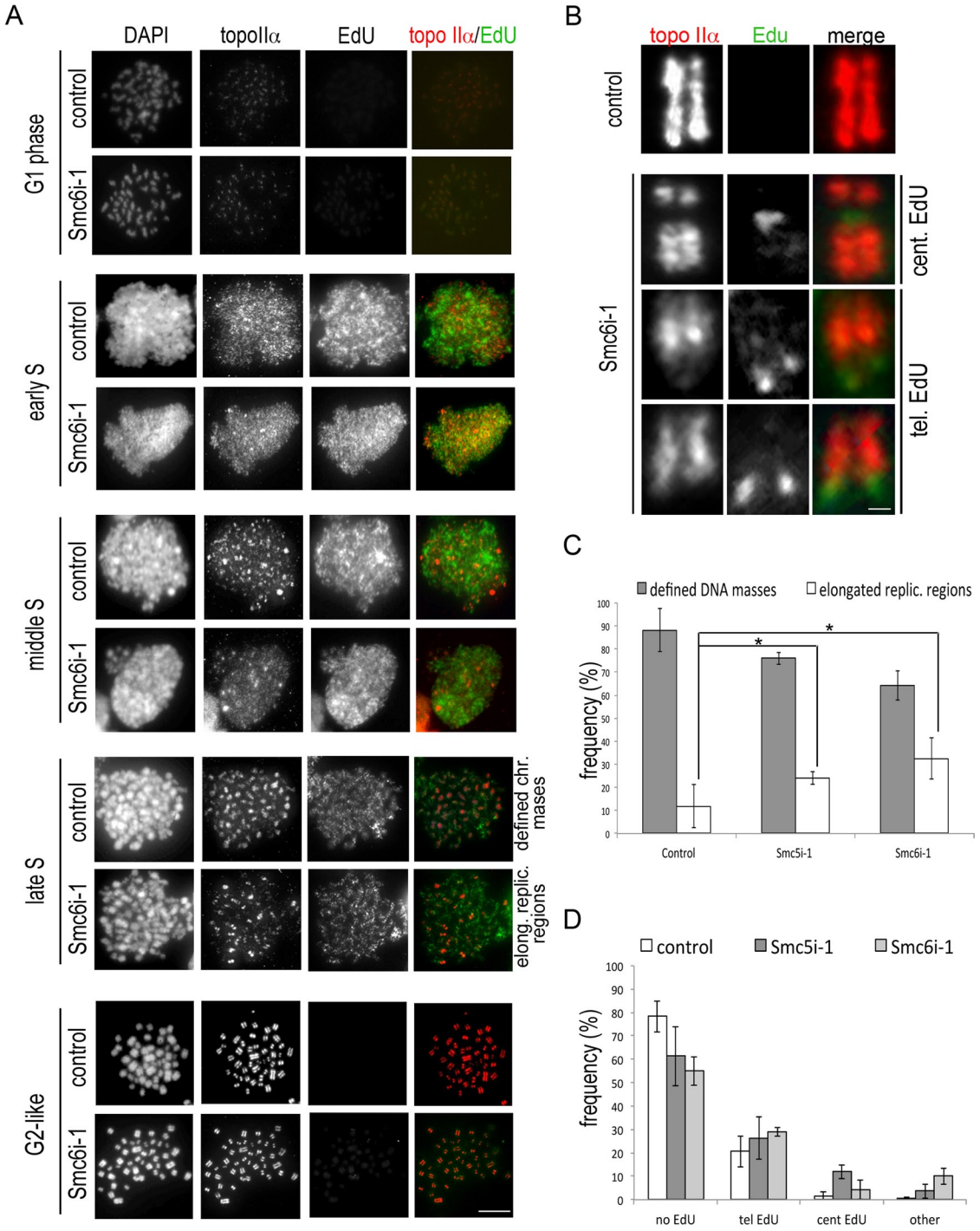

FIGURE 9: Progression of DNA replication and loading of topo IIα onto sister chromatids in S phase. (A) PCC analysis with EdU pulse-labeling was carried out as described in Figure 8, E and F. Immunofluorescence microscopy images of DNA (DAPI), topo IIα (red in merged images), and EdU (green) are shown. Note that late S phase can be characterized based on two properties: elongated replicating regions and well-defined chromatin masses. Right panels show merged EdU and topo IIα staining. Scale bar: 10 μm. (B) Frequently observed G_2-like chromosomes in Smc6 siRNA–treated cells. Note that EdU-positive extended regions of ongoing replication (green) exclude topo IIα axial localization (red). Right panels show merged images. Scale bar: 1 μm. (C) The elongated replicating regions are more often seen in late S phase of Smc5/6-depleted cells. PCC-induced late S-phase cells are assessed for the completion of DNA replication by counting the incidence of elongated replicating regions and defined chromatin masses. (D) Frequency of PCC-induced nuclei at G_2 showing persistent EdU staining. One hundred metaphases were analyzed for each sample in (C) and (D). Bar graph shows mean ± SD from three independent experiments; p value < 0.05; *, $p = 0.010.05$; two-tailed Student's t test.

expression. Determining the prospective function of Smc5/6 in G_1 phase and how cohesin and Smc5/6 might coordinate to shape chromatin awaits further investigations.

Chromosomal recruitment of topo IIα depends on Smc5/6

Our data suggest that the function of Smc5/6 is essential to form an intact axial structure of mitotic chromosomes. Instead of being enriched at centromeres, topo IIα tended to accumulate at the distal arms in Smc5- and Smc6-depleted cells (Figure 4). Moreover, ChIP-Seq analysis revealed that the chromosomal binding profile of topo IIα is not drastically changed by Smc6 depletion in interphase, albeit a lesser amount of chromatin-bound protein was detected under this conditions. By contrast, the redistribution of the protein from interphase binding sites to the centromeric region in mitosis is blocked in Smc6-depleted cells (Figure 6). We could reason that this defective relocalization of topo IIα caused characteristic uneven condensation between the chromosomal arms and centromeres in the absence of Smc5/6.

How might Smc5/6 regulate topo IIα recruitment to chromosomes? Previous study in *Xenopus* egg extracts indicated that DNA replication allows topo IIα to be tightly associated with chromosomes, such that it becomes detectable at the chromosomal axial structure (Cuvier and Hirano, 2003). In agreement with this, our PCC assay indicated that topo IIα association with chromatin increases as replication progresses, and topo IIα's accumulation at chromosome axes became unambiguously detectable after replication and sister chromatid pairs were formed (Figure 9). Moreover, visualization of the nascent DNA by EdU pulse-labeling revealed that regions of active replication always excluded topo IIα accumulation (Figure 9). These observations are consistent with the idea that the topo IIα–mediated subchromosomal axis construction is intimately coupled to the process of DNA replication. This would explain why defective replication processing in the absence of Smc5/6 disturbs the correct timing of topo IIα deposition, which results in lesser amounts of topo IIα bound to chromatin (Figure 6).

Supporting the hypothesis that topo IIα–mediated axial structure plays a crucial role in organizing chromosomes, a wide range of aberrant chromosome structures, including curly axes, fused telomeres, and double-axes, were induced by Smc5/6 depletion (Figure 5). These structures were found to be associated with abnormal distribution of condensin, which would reflect disorganized chromosomal axes caused by improper deposition of topo IIα. However, it was recently found that condensin II promotes structural reorganization of duplicated chromosomes immediately after replication (Ono *et al.*, 2013). Thus a direct interplay between condensin and Smc5/6 during DNA replication to coordinate chromosome assembly may also exist.

Smc5/6 links DNA replication to chromosome segregation

The fact that Smc5/6-depleted cells exhibited increased levels of replication-related DNA damage indicates that replication fork stalling and/or collapse occur frequently in these cells and that these conditions directly relate to the slower processing of DNA replication (Figures 7 and 9), a notion consistent with previous observations in yeast (Torres-Rosell *et al.*, 2007; Bermúdez-López *et al.*, 2010). Significantly, the frequency of the damage, as well as the curly chromosomal phenotype and the abnormal axial staining of topo IIα, were markedly reduced when cells were subjected to G_2 arrest and thereby allowed extra time to complete DNA replication before mitosis (Figure 8, C–E). It is therefore conceivable that the aberrant chromosome morphology in Smc5/6-depleted cells is directly related to a temporal disconnection between DNA replication and chromosome assembly. Smc5/6 function could be also involved in the DNA damage checkpoint control, as has been proposed in yeasts (Verkade *et al.*, 1999; Chen *et al.*, 2013), in which case Smc5/6 inactivation should deteriorate the temporal disconnection.

Our work suggests a model in which the Smc5/6 complex regulates replication fork progression and the replication-dependent reorganization of topo IIα distribution along chromosomes before cells enter mitosis. An important implication of these observations is that replication progression can directly affect chromosome assembly in mitosis. Relocalization of topo IIα from interphase to mitotic binding sites would be a major event for the structural transition of chromosomes during the cell cycle, and an obvious follow-up study is to explore the mechanistic basis for this. We can speculate that the existence of DNA linkages that arose from stalled/collapsed replication forks impede the dynamic interaction and positioning of topo IIα on chromatin.

Delayed or incomplete replication within repetitive sequences, such as the ribosomal DNA loci or telomeric regions, is a common feature of Smc5 and Smc6 deficiency in other systems and results in chromosome missegregation (Torres-Rosell *et al.*, 2005; Chavez *et al.*, 2010). Similarly, we found that Smc5- and Smc6-depleted human cells contained persistent active replication at centromeres and telomeres, which resulted in intertwining and linkages between sister chromatids in mitotic chromosomes. Both centromeres and telomeres are known as late-replicating regions in human cells, and the timing of DNA replication and the subsequent chromatin assembly at these domains may therefore be challenged in the context of replication stress. It is tempting to speculate that the function of Smc5/6 becomes particularly crucial in maintaining the stability of late-replicating regions in human genome.

MATERIALS AND METHODS

Antibodies

Antibody to Smc2 was generously provided by Jan-Michael Peters (Research Institute of Molecular Pathology, Vienna, Austria). A mouse monoclonal antibody was raised against the peptide sequence MATPSKKTSTPSPQPSKRALPRDPSSEVPC of Smc5 (Monoclonal Antibody Research Institute, Sapporo, Japan) and then purified using a protein G affinity column (MabTrap kit; Amersham Biosciences, Piscataway, NJ). Antibodies against other proteins were as follows: SMC6L1 (M01, Cl7one 2E6; Abnova, Taipei, Taiwan), Smc6 (sc-365742, clone A-3; Santa Cruz Biotechnology, Santa Cruz, CA), SMC5 (18038; Abcam, Cambridge, UK), BLM (sc-7790, Santa Cruz Biotechnology), PICH (Clone 142-26-3; Millipore, Billerica, MA), DNA topoisomerase IIα (D081-1, clone 8D2; MBL, Aichi, Japan), DNA topoisomerase IIα (74715; Abcam), cyclin B (610219; BD PharMingen, Lexington, KY), α-tubulin (T6074, clone B-5-1-2; Sigma-Aldrich, St. Louis, MO), GFP (290; Abcam), and phospho–histone H3 (Ser-10) (9701; Cell Signaling Technology, Danvers, MA), cyclin B1 (K0128-3, clone V152; MBL), phospho–histone H3 (Ser-10) (9706, clone 6G3; Cell Signaling Technology), histone H2B (ab1790; Abcam), and γ-H2AX (A300-081A; Bethyl, Montgomery, TX).

Chromatin fractionation

For isolation of chromatin, cells were resuspended (4×10^7 cells/ml) in buffer A (10 mM HEPES, pH 7.9, 10 mM KCl, 1.5 mM $MgCl_2$, 0.34 M sucrose, 10% glycerol, 1 mM dithiothreitol [DTT], 5 μg/ml aprotinin, 5 μg/ml leupeptin, 0.5 μg/ml pepstatin A, 0.1 mM phenylmethylsulfonyl fluoride). Triton X-100 (0.1%) was added, and the cells were incubated for 5 min on ice. Nuclei were pelleted by

low-speed centrifugation (5 min, 1590 × *g*, 4°C). The supernatant containing the cytoplasmic fraction was further clarified by high-speed centrifugation (15 min, 3977 × *g*, 4°C) to remove cell debris and insoluble aggregates. Nuclei were washed once and then resuspended in buffer A containing Triton X-100 (0.1%) and analyzed by immunoblotting.

Cell synchronization, inhibitor treatment, and cell lines

HeLa and RPE-1 cells were cultured in DMEM (Wako, Tokyo, Japan) supplemented with 10% fetal calf serum (FBS; Equitech-Bio, Tokyo, Japan), 0.2 mM L-glutamine, 100 U/ml penicillin, and 100 µg/ml streptomycin (Meiji Seika, Tokyo, Japan) at 37°C in a 5% CO_2 environment. HeLa cells were synchronized by double thymidine arrest (24 h in the presence of 2 mM thymidine [T1895–1G; Sigma-Aldrich], 8 h release, 12 h in the presence of 2 mM thymidine) and were collected every 3 h after the second release for cell cycle progression analysis.

RPE-1 cells were synchronized at G_0/G_1 by serum starvation for 96 h and then released into the cell cycle with fresh medium containing 10% fetal calf serum for further analysis. For G_2/M-phase arrest, asynchronous RPE-1 cells were treated with 9.0 µM RO-3306 (Enzo Life Sciences, Plymouth, PA) for 12 or 24 h. For enrichment of cells in prometaphase, 50 ng/ml nocodazole was added 7 h after release from the second thymidine block for 1 or 2 h; RPE-1 cells were treated with 15 mM STLC (TCI, Tokyo, Japan) for 2 h after release from RO-3306 arrest or 31 h after release from serum starvation for 2 or 3 h, and then recovered by mitotic shake-off. The HeLa cell line stably expressing EGFP-tagged Smc5 protein was generated by fusing EGFP in frame with the C terminus of Smc5 in a bacterial artificial chromosome vector (clone RP11; BACPAC Resources, Oakland, CA). The plasmid DNA was purified and transfected into HeLa cells using the FuGENE 6 reagent (Promega, Madison, WI). Stably expressing cell clones were selected in a complete medium containing G418, and expression of the tagged transgene was verified by fluorescence microscopy and immunoblotting. For visualization of regions with newly synthesized DNA, cells were cultured in medium supplemented with 10 µM EdU kit (Invitrogen, Carlsbad, CA) for 0.5 h before fixation.

PCC assay

PCC was induced by adding calyculin A (Wako) into culture media at a final concentration of 160 nM. After 1 h, cells were hypotonically swollen in a 40:60 mix (vol/vol) of phosphate-buffered saline (PBS) and distilled water for 5 min at room temperature. Cells were fixed with freshly made Carnoy's solution (70% methanol, 30% acetic acid), dropped on glass slides, and dried. Slides were stained with 5% Giemsa stain, washed with water, air-dried, and mounted with Entellan embedding agent (Merck, Darmstadt, Germany). For detection of incorporated EdU, the Click-iT EdU imaging kit (Invitrogen) was used. Briefly, the glass slides were incubated with a reaction solution containing fluorochrome-azide (Alexa Fluor 488) for 1 h at room temperature, after which immunofluorescence staining was conducted.

RNA interference

siRNA sequences were as follows: Smc5 siRNA-1, 5′-GGAACUUCAGCAGGGCUUUAAUAGUA-3′; Smc5 siRNA-2, 5′-GGCAUUAUGUGAAGGCGAAAUAAUU-3′; Smc6 siRNA-1, 5′-CAAAUUCUUCAUGAAAGCAACGCAA-3′; Smc6 siRNA-2, 5′-GACCUAUCUUGAUCUGGAUAGUAAA-3′. Smc6 siRNA-1 was used for ChIP-Seq analysis of topo IIα. Cells were transfected by incubating 50 nM duplex siRNA with Lipofectamine RNAiMAX (Invitrogen) in antibiotic-free growth medium. RNA interference (RNAi) was performed concomitantly with the synchronization with thymidine or serum starvation, and 48 h of transfection with each siRNA was required for maximal knockdown of Smc5 and Smc6. For control transfections, the same annealing reaction was set up without the presence of siRNA oligonucleotides.

Chromosome spreads

RPE-1 cells treated with STLC (15 mM) for 2–3 h were collected by mitotic shake-off and hypotonically swollen in a 40:60 mix (vol/vol) of PBS and distilled water for 5 min at room temperature. Cells were fixed with freshly made Carnoy's solution, dropped on glass slides, and dried. Slides were stained with 5% Giemsa stain, washed with water, air-dried, and mounted with Entellan embedding agent.

Immunofluorescence microscopy

Cells grown on coverslips with or without preextraction with 0.2% PBS/Tween 100 were fixed with ice-chilled 100% methanol for 20 min at –20°C or with 4% paraformaldehyde in 0.137 M sodium phosphate buffer (pH 7.4). Fixed cells/chromosomes were permeabilized with 0.5% Triton X-100 in PBS and incubated with 3% bovine serum albumin in PBS for at least 1 h. Cells were incubated with the primary antibodies overnight at room temperature; this was followed by incubation with secondary antibodies for 35 min together with 0.1 µg/ml 4,6-diamidino-2-phenylindole (DAPI). The secondary antibodies used in this study were goat anti-rabbit immunoglobulin G (IgG) and goat anti-mouse IgG coupled to Alexa Fluor 488 or 568 and goat anti-human IgG coupled to Alexa Fluor 568 (Molecular Probes, Carlsbad, CA). Cells were washed twice and mounted in ProLong Gold anti-fade mounting reagent (Invitrogen). Images were acquired on a Zeiss Imager Z.1 microscope equipped with epifluorescence and a CoolSNAP HQ CCD camera (Photometrics, Tucson, AZ). Three-dimensional projections of the immunofluorescence images were carried out using the 3D Volume viewer tool in ImageJ software (National Institutes of Health, Bethesda, MD).

Live-cell imaging analysis

Cells were placed in CO_2-independent medium without phenol red (Life Technologies-BRL, Grand Island, NY) on chambered coverslips (Lab-Tek; Nunc, Rochester, NY), and the chamber lids were sealed with silicone grease. Images were captured every 3 min, with 100-ms exposure times, through a 100×/1.40 NA Plan-Apochromat oil-objective lens mounted on an inverted microscope (IX-71; Olympus, Tokyo, Japan) equipped with a CoolSNAP HQ CCD camera. A series of projected images of three Z-sections with 5.0-µm intervals were analyzed. For data analysis, images were processed using ImageJ software.

Immunoprecipitation

Asynchronized HeLa cells expressing EGFP-tagged Smc5 were lysed in immunoprecipitation buffer (20 mM Tris-HCl, pH 7.5, 150 mM NaCl, 20 mM β-glycerophosphate, 5 mM $MgCl_2$, 0.1% NP-40, protease inhibitors [Complete Mini EDTA-free; Roche, Indianapolis, IN], 1 mM DTT), supplemented with 100 nM okadaic acid, 2 mM Na_3VO_4, 10 mM NaF, and 0.25 U/l benzonase nuclease (Novagen, EMD Millipore, Billerica, MA), for 20 min on ice. Cell extracts, after the insoluble fraction was removed by centrifugation at 15,000 rpm for 30 min at 4°C, were used for immunoprecipitation. Ten microliters of protein A (Bio-Rad, Hercules, CA) beads coupled to antibodies was incubated with cell extracts for ~2 h at 4°C and then washed

three times with immunoprecipitation buffer and three times with 0.05% TBS-Tween20.

Fluorescence-activated cell sorting analysis

Cells were harvested by trypsinization, fixed in 70% ethanol, stained with propidium iodide solution at a final concentration of 50 μg/ml, and subjected to fluorescence-activated cell sorting (FACS) analysis on FaCScalibur using Cell Quest (Becton Dickinson, Mansfield, MA) software.

ChIP

Cells were cross-linked with 1% formaldehyde for 10 min, quenched with 125 mM glycine, and prepared for ChIP as previously described (Wendt *et al.*, 2008). ChIP was performed as previously described using SMC6L1 (M01, Cl7one 2E6; Abnova) and DNA topoisomerase IIα (D081-1, clone 8D2; MBL; Wendt *et al.*, 2008). In brief, cross-linked cell lysates solubilized by sonication were incubated with Affi-prep protein A Support (Bio-Rad) and cross-linked with the antibodies for 14 h at 4°C. After this, beads were washed several times and eluted with elution buffer (50 mM Tris, 10 mM EDTA, and 1% SDS) for 20 min at 65°C. The eluates were incubated at 65°C overnight to reverse cross-links and were then treated with RNaseA and then with proteinase K. The samples were further purified by phenol–chloroform extraction and an extra purification step using a PCR purification kit (Qiagen, Valencia, CA).

ChIP-Seq analyses

DNA from whole-cell extracts (WCE) and ChIP fractions was further sheared by sonication (Branson sonifier 250D), end-repaired, ligated to sequencing adaptors, and amplified according to the SOLiD Library Preparation kit Protocol (Applied Biosystems, Foster City, CA). DNA purified from gel and amplified between 100 and 150 base pairs was sequenced on the Applied Biosystems SOLiD platforms (SOLiD 3 and 5500) to generate single-end 50–base pair reads. Sequenced data for both ChIP fractions and WCE were aligned to the human genome (UCSC hg19) using Bowtie (Langmead *et al.*, 2009), allowing three mismatches in the first 28 bases per read (-n3 option). Software DROMPA was used for visualization and statistical analysis of ChIP-Seq data sets (Nakato *et al.*, 2013). All duplicate reads and those without unique alignment were removed from further analysis. ChIP-Seq and DNA sequencing data from this study have been deposited in the Sequence Read Archive database (www.ncbi.nlm.nih.gov/sra) under accession number SRX381015. We further analyzed only uniquely aligned reads. Each aligned read was extended to a predicted fragment length of 150 base pairs. Reads were summed in 100-kb windows along the chromosome, and the fold enrichment (ChIP/WCE) for each window was calculated.

Raw data availability

Original unprocessed versions of all figures have been uploaded to the server of IMCB, the University of Tokyo, and are available on request.

ACKNOWLEDGMENTS

We are grateful to Jan-Michael Peters (Research Institute of Molecular Pathology, Vienna) for the Smc2 antibody. This work was supported by grants from the Research Program of Innovative Cell Biology by Innovative Technology, Ministry of Education, Culture, Sports and Technology of Japan; the Grant-in-Aid for Scientific Research (S) program of the Japan Society for the Promotion of Science; and the Cell Science Research Foundation.

REFERENCES

Ampatzidou E, Irmisch A, O'Connell MJ, Murray JM (2006). Smc5/6 is required for repair at collapsed replication forks. Mol Cell Biol 26, 9387–9401.

Baumann C, Korner R, Hofmann K, Nigg EA (2007). PICH, a centromere-associated SNF2 family ATPase, is regulated by Plk1 and required for the spindle checkpoint. Cell 128, 101–114.

Bermúdez-López M, Ceschia A, de Piccoli G, Colomina N, Pasero P, Aragon L, Torres-Rosell J (2010). The Smc5/6 complex is required for dissolution of DNA-mediated sister chromatid linkages. Nucleic Acids Res 38, 6502–6512.

Chavez A, George V, Agrawal V, Johnson FB (2010). Sumoylation and the structural maintenance of chromosomes (Smc) 5/6 complex slow senescence through recombination intermediate resolution. J Biol Chem 285, 11922–11930.

Chen Y-H, Szakal B, Castellucci F, Branzei D, Zhao X (2013). DNA damage checkpoint and recombinational repair differentially affect the replication stress. Mol Biol Cell 24, 2431–2441.

Chiolo I, Minoda A, Colmenares SU, Polyzos A, Costes SV, Karpen GH (2011). Double-strand breaks in heterochromatin move outside of a dynamic HP1a domain to complete recombinational repair. Cell 144, 732–744.

Cuvier O, Hirano T (2003). A role of topoisomerase II in linking DNA replication to chromosome condensation. J Cell Biol 160, 645–655.

Davalos AR, Campisi J (2003). Bloom syndrome cells undergo p53-dependent apoptosis and delayed assembly of BRCA1 and NBS1 repair complexes at stalled replication forks. J Cell Biol 162, 1197–1209.

DeBonis S *et al.* (2004). In vitro screening for inhibitors of the human mitotic kinesin Eg5 with antimitotic and antitumor activities. Mol Cancer Ther 3, 1079–1090.

De Piccoli G *et al.* (2006). Smc5-Smc6 mediate DNA double-strand-break repair by promoting sister-chromatid recombination. Nat Cell Biol 8, 1032–1034.

Earnshaw WC, Halligan B, Cooke CA, Heck MMS, Liu LF (1985). Topoisomerase II is a structural component of mitotic chromosome scaffolds. J Cell Biol 100, 1706–1715.

Fujioka Y, Kimata Y, Nomaguchi K, Watanabe K, Kohno K (2002). Identification of a novel non-structural maintenance of chromosomes (SMC) component of the SMC5–SMC6 complex involved in DNA repair. J Biol Chem 277, 21585–21591.

Gasser SM, Laroche T, Falquet J, Boy de la Tour E, Laemmli UK (1986). Metaphase chromosome structure. Involvement of topoisomerase II. J Mol Biol 188, 613–629.

Gerlich D, Hirota T, Koch B, Peters JM, Ellenberg J (2006). Condensin I stabilizes chromosomes mechanically through a dynamic interaction in live cells. Curr Biol 16, 333–344.

Gomez T, Jordan PW, Viera A, Alsheimer M, Fukuda T, Jessberger R, Llano E, Pendas AM, Handel MA, Suja JA (2013). Dynamic localization of SMC5/6 complex proteins during mammalian meiosis and mitosis suggests functions in distinct chromosome processes. J Cell Sci 126, 4239–4252.

Harvey SH, Sheedy DM, Cuddihy AR, O'Connell MJ (2004). Coordination of DNA damage responses via the Smc5/Smc6 complex. Mol Cell Biol 24, 662–674.

Hirano T (2002). The ABCs of SMC proteins: two-armed ATPases for chromosome condensation, cohesion, and repair. Genes Dev 16, 399–414.

Hirano T, Kobayashi R, Hirano M (1997). Condensins, chromosome condensation protein complexes containing XCAP-C, XCAP-E and a *Xenopus* homolog of the *Drosophila* Barren protein. Cell 89, 511–521.

Hirano T, Mitchison TJ (1994). A heterodimeric coiled-coil protein required for mitotic chromosome condensation in vitro. Cell 79, 449–458.

Irmisch A, Ampatzidou E, Mizuno K, O'Connell MJ, Murray JM (2009). Smc5/6 maintains stalled replication forks in a recombination-competent conformation. EMBO J 28, 144–155.

Kegel A, Betts-Lindroos H, Kanno T, Jeppsson K, Ström L, Katou Y, Itoh T, Shirahige K, Sjögren C (2011). Chromosome length influences replication-induced topological stress. Nature 471, 392–396.

Langmead B, Trapnell C, Pop M, Salzberg SL (2009). Ultrafast and memory-efficient alignment of short DNA sequences to the human genome. Genome Biol 10, R25.

Lehmann AR, Walicka M, Griffiths DJF, Murray JM, Watts FZ, McCready S, Carr AM (1995). The rad18 gene of *Schizosaccharomyces pombe* defines a new subgroup of the SMC superfamily involved in DNA repair. Mol Cell Biol 15, 7067–7080.

Li W, Kim SM, Lee J, Dunphy WG (2004). Absence of BLM leads to accumulation of chromosomal DNA breaks during both unperturbed and disrupted S phases. J Cell Biol 165, 801–812.
Lindroos HB, Ström L, Itoh T, Katou Y, Shirahige K, Sjögren C (2006). Chromosomal association of the Smc5/6 complex reveals that it functions in differently regulated pathways. Mol Cell 22, 755–767.
Losada A, Hirano M, Hirano T (1998). Identification of *Xenopus* SMC protein complexes required for sister chromatid cohesion. Genes Dev 12, 1986–1997.
Maeshima K, Laemmli UK (2003). A two-step scaffolding model for mitotic chromosome assembly. Dev Cell 4, 467–480.
McDonald WH, Pavlova Y, Yates JR, III, Boddy MN (2003). Novel essential DNA repair proteins Nse1 and Nse2 are subunits of the fission yeast Smc5–Smc6 complex. J Biol Chem 278, 45460–45467.
Morikawa H, Morishita T, Kawane S, Iwasaki H, Carr AM, Shinagawa H (2004). Rad62 protein functionally and physically associates with the Smc5/Smc6 protein complex and is required for chromosome integrity and recombination repair in fission yeast. Mol Cell Biol 24, 9401–9413.
Nakato R, Itoh T, Shirahige K (2013). DROMPA: easy-to-handle peak calling and visualization software for the computational analysis and validation of ChIP-seq data. Genes Cells 18, 589–601.
Ono T, Yamashita D, Hirano T (2013). Condensin II initiates sister chromatid resolution during S phase. J Cell Biol 200, 429–441.
Outwin EA, Irmisch A, Murray JM, O'Connell MJ (2009). Smc5-Smc6-dependent removal of cohesin from mitotic chromosomes. Mol Cell Biol 29, 4363–4375.
Pebernard S, McDonald WH, Pavlova Y, Yates JRIII, Boddy MN (2004). Nse1, Nse2, and a novel subunit of the Smc5–Smc6 complex, Nse3, play a crucial role in meiosis. Mol Biol Cell 15, 4866–4876.
Potts PR, Porteus MH, Yu H (2006). Human SMC5/6 complex promotes sister chromatid homologous recombination by recruiting the SMC1/3 cohesin complex to double-strand breaks. EMBO J 25, 3377–3388.
Rouzeau S, Cordelières FP, Buhagiar-Labarchède G, Hurbain I, Onclercq-Delic R, Gemble S, Magnaghi-Jaulin L, Jaulin C, Amor-Guéret M (2012). Bloom's syndrome and PICH helicases cooperate with topoisomerase IIα in centromere disjunction before anaphase. PLoS One 7, e33905.
Shimura T, Torres MJ, Martin MM, Rao VA, Pommier Y, Katsura M, Miyagawa K, Aladjem MI (2008). Bloom's syndrome helicase and Mus81 are required to induce transient double-strand DNA breaks in response to DNA replication stress. J Mol Biol 375, 1152–1164.
Spence JM, Phua HH, Mills W, Carpenter AJ, Porter AC, Farr CJ (2007). Depletion of topoisomerase IIα leads to shortening of the metaphase interkinetochore distance and abnormal persistence of PICH-coated anaphase threads. J Cell Sci 120, 3952–3964.
Stephan AK, Kliszczak M, Dodson H, Cooley C, Morrison CG (2011). Roles of vertebrate Smc5 in sister chromatid cohesion and homologous recombinational repair. Mol Cell Biol 31, 1369–1381.
Sumara I, Vorlaufer E, Gieffers C, Peters BH, Peters JM (2000). Characterization of vertebrate cohesin complexes and their regulation in prophase. J Cell Biol 151, 749–762.
Taylor EM, Moghraby JS, Lees JH, Smit B, Moens PB, Lehmann AR (2001). Characterization of a novel human SMC heterodimer homologous to the *Schizosaccharomyces pombe* Rad18/Spr18 complex. Mol Biol Cell 12, 1583–1594.
Torres-Rosell J, De Piccoli G, Cordon-Preciado V, Farmer S, Jamuz A, Machin F, Pasero P, Lisby M, Haber JE, Aragon L (2007). Anaphase onset before complete DNA replication with intact checkpoint responses. Science 315, 1411–1415.
Torres-Rosell J, Machin F, Farmer S, Jarmuz A, Eydmann T, Dalgaard JZ, Aragon L (2005). SMC5 and SMC6 genes are required for the segregation of repetitive chromosome regions. Nat Cell Biol 7, 412–419.
Toth A, Ciosk R, Uhlmann F, Galova M, Schleiffer A, Nasmyth K (1999). Yeast cohesin complex requires a conserved protein, Eco1p(Ctf7), to establish cohesion between sister chromatids during DNA replication. Genes Dev 13, 320–333.
Tsuyama T, Inou K, Seki M, Seki T, Kumata Y, Kobayashi T, Kimura K, Hanaoka F, Enomoto T, Tada S (2006). Chromatin loading of Smc5/6 is induced by DNA replication but not by DNA double-strand breaks. Biochem Biophys Res Commun 351, 935–939.
Uemura T, Ohkura H, Adachi Y, Morino K, Shiozaki K, Yanagida M (1987). DNA topoisomerase II is required for condensation and separation of mitotic chromosomes in *S. pombe*. Cell 50, 917–925.
Uhlmann F, Lottspeich F, Nasmyth K (1999). Sister-chromatid separation at anaphase onset is promoted by cleavage of the cohesin subunit Scc1. Nature 400, 37–42.
Uhlmann F, Wernic D, Poupart M-A, Koonin EV, Nasmyth K (2000). Cleavage of cohesin by the CD clan protease separin triggers anaphase in yeast. Cell 103, 375–386.
Verkade HM, Bugg SJ, Lindsay HD, Carr AM, O'Connell MJ (1999). Rad18 is required for DNA repair and checkpoint responses in fission yeast. Mol Biol Cell 10, 2905–2918.
Wendt KS *et al*. (2008). Cohesin mediates transcriptional insulation by CCCTC-binding factor. Nature 451, 796–801.
Wu N, Kong X, Ji Z, Zeng W, Potts PR, Yokomori K, Yu H (2012). Scc1 sumoylation by Mms21 promotes sister chromatid recombination through counteracting Wapl. Genes Dev 26, 1473–1485.